An Approach to Simulate the Motion of 2- and 3-dimensional Fuel Particles in Combustion Chambers

A. Džiugys, B. Peters

Institut für Kern- und Energietechnik
Programm Nachhaltigkeit, Energie- und Umwelttechnik

März 2002

An Approach to Simulate the Motion of 2- and 3-dimensional Fuel Particles in Combustion Chambers

A. Džiugys, B. Peters

Abstract

The objective of the present work is to identify and implement a numerical method that can deal with the motion of a packed bed of fuel particles in combustion chambers such as a grate furnace and a rotary kiln. As a result of an extensive review of the various numerical methods applied in the areas of granular matter and molecular dynamics a time driven approach was found to be suited to the numerical simulation of particle motion in combustion chambers. Furthermore, this method can also be employed to deal with moving boundaries which are required for the present application e.g. travelling grate. The method works in a Lagrangian frame of reference which uses the position and orientation of particles as independent variables. These are obtained by time integration of the three-dimensional dynamics equations, derived from the classical Newtonian approach for each particle. This includes keeping track of all the forces and momentums acting on each particle at every time step. Visco-elastic contact forces include normal and tangential components with visco-elastic models for energy dissipation and friction. The particle shapes are approximated by spheres and ellipsoids, whereby a varying size and ratio of the semi-axis accounts for the variety of particle geometries in a combustion chamber. For these shapes, the overlap of particles during contact is expressed by an polynomial of 4th order for two-dimensional case, and an polynomial of 6th order for three-dimensional case. A new algorithm to detect the two-dimensional elliptical particles contact sufficiently accurate was developed. It is based on a sequence of coordinate transformations and has proved its reliability in numerous applications. Finally, the method was applied to simulate the motion of spherical and elliptical particles in a rectangular enclosure, on a travelling grate and in a rotary kiln.

1

Eine Methode zur Simulation der Bewegung von 2- und 3-dimensionalen Brennstoffpartikeln in Brennkammern

Zusammenfassung

Die Zielsetzung der vorliegenden Arbeit war die Identifikation und die Implementierung einer numerischen Methode, die die Bewegung von Brennstoffpartikeln in Brennkammern wie auf dem Rost oder im Drehrohr simulieren kann. Als Ergebnis einer extensiven Literaturrecherche über vielfältige Methoden aus dem Gebiet der Bewegung von granularen Medien und der Molekulardynamik wurde ein zeitschrittgesteuerter Algorithmus als anwendbar für die Simulation der Bewegung von Brennstoffpartikeln in Brennkammern beurteilt. Weiterhin kann die Methode mit bewegten Rändern umgehen, welche für die vorliegende Anwendung eines Vorschubrostes benötigt werden. Die Methode ist in einen Lagrange System formuliert, welches die Position und die Orientierung der Partikel als unabhängige Variablen benutzt. Sie ergeben sich aus der Zeitintegration der dreidimensionalen Newtonschen Bewegungsgleichungen für jedes Partikel. Dazu müssen Kräfte und Momente, die an den Partikel angreifen, für jeden Zeitschritt bestimmt werden. Die viskoelastischen Konta ktkräfte beinhalten normale und tangentiale Komponenten mit Dissipation und Reibung. Die Partikelformen werden durch Kreise, Kugeln und Ellipsen approximiert, wobei ein variables Verhältnis der Halbachsen die Vielfalt der verschiedenen Partikelformen in einer Brennkammer berücksichtigt. Für die zweidimensionalen Geometrien wird die Überlappung durch ein Polynom 4. Grades ausgedrückt, während sich für den dreidimensionalen Fall ein Polynom 6. Grades ergibt. Zur Bestimmung der Überlappung von zweidimensionalen Partikeln wurde ein neuer Algorithmus entwickelt. Er basiert auf einer Sequenz von Koordinatentransformationen und hat sowohl seine Genauigkeit als auch seine Zuverlässigkeit in vielen Anwendungen bewiesen. Mit dieser Methode wurden Anwendungen von kreisförmigen und elliptischen Partikeln in einer Schleuse, auf einen Vorschubrost und im Drehrohr berechnet.

Contents

List of Tables

4

List of Figures

1 Introduction

Figure 1: Burning of waste in a packed bed

Technical applications involving a packed bed of particles (Fig. 1) are frequently used in the processing industry, energy-supplying industry and in waste incineration plants. Common to all these applications is that the entire flow and combustion process consists of several important thermodynamic and fluid dynamic processes, among which are the motion of the packed bed with its redistribution of particles and the chemical conversion processes of heterogeneous combustion. The packed bed can be described as granular material which can be idealised as an ensemble of a large number of particles.

For the simulation of the motion of fuel particles on a grate or in a rotary kiln a time driven approach was employed. Due to its application in combustion devices the size of the particles was chosen to be in the range of cm. In a first approach 2-dimensional circular and elliptical particles were used

7

in the predictions, because the overlap between particles is determined by a numerically stable algorithm. Furthermore, the approximation of the motion in a rotary kiln or on a grate in a relevant plane with 2-dimensional particles is sufficiently accurate for technical applications. However, the method is already extended to the packing of 3-dimensional spherical soot particles.

2 Description of the Model

Below we will describe shortly the method what we chose to simulate the motion of granular material. A time-driven method, which takes into account all forces and torques acting on a particle being in contact with neighbours at any time, was identified as the most favourable approach for numerical simulation of the motion of fuel particles in combustion chambers (Džiugys and Peters, 1998).

However, most of the reviewed applications deal with spherical particles. It is not sufficient to represent the various shapes of fuel particles in a combustion chamber. Therefore, in a first approach an elliptical geometry was chosen to represent a large variety of shapes by different sizes and ratios of the semi-axis, thus extending the circular shapes. Consequently, an algorithm to determine the two-dimensional overlap of elliptical particles accurately and reliably has to be developed, which is described here. Final applications of the method proofs its suitability to the application in combustion chambers.

The time-driven method was used to simulate the behaviour of granular material, which means that an impact between particles is approximated by a representative overlap area or volume of particle shapes in the vicinity of the point of impact as shown in Fig. 2.
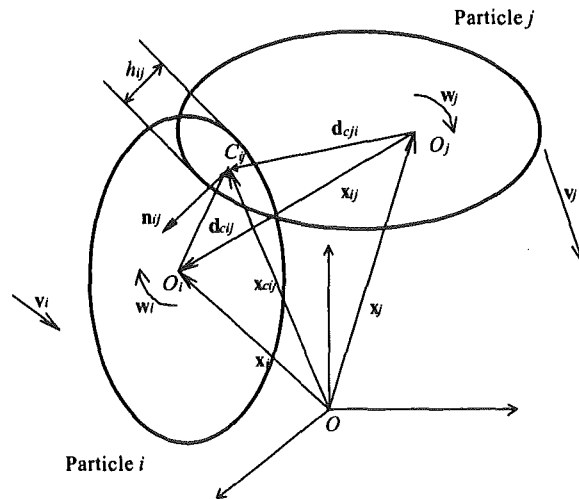
Figure 2: Geometry of overlapping contact of two elastic particles

9

The state of all particles, at the time t, are updated after fixed time step Δt, which is smaller than the smallest time of impact. The motion of each particle in the granular material is described by the second Newton law

$$m_i \frac{d^2 \mathbf{x}_i}{dt^2} = m_i \mathbf{a}_i = \mathbf{F}_i \tag{1}$$

$$\mathbf{v}_i = \frac{d\mathbf{x}_i}{dt} \tag{2}$$

$$I_i \frac{d^2 \boldsymbol{\theta}_i}{dt^2} = I_i \mathbf{u}_i = \mathbf{T}_i \tag{3}$$

$$\mathbf{w}_i = \frac{d\boldsymbol{\theta}_i}{dt} \tag{4}$$

where $\mathbf{v}_i$, $\mathbf{a}_i$, $\mathbf{x}_i$, $\mathbf{w}_i$, $\mathbf{u}_i$ and $\boldsymbol{\theta}_i$ are vectors of velocity, acceleration, position, angular velocity, acceleration and orientation of the centre of gravity m_i of the particle i ($i=[1,N]$), N is the number of particles in the granular material. I_i is the inertial tensor of the particle. $\mathbf{F}_i$ and $\mathbf{T}_i$ are the sum of all forces and torques, respectively, which act on the particle i. External forces and the fluid influence were neglected. Therefore, $\mathbf{F}_i = m_i \mathbf{g} + \mathbf{F}_{i,contact}$ and $\mathbf{T}_i = \mathbf{T}_{i,contact}$, where $\mathbf{F}_{i,contact}$ is the summation of direct contact forces between the particle i and another $N-1$ particle

$$\mathbf{F}_{i,contact} = \sum_{j=1, j \neq i}^{N} \mathbf{F}_{ij} \tag{5}$$

where $\mathbf{F}_{ij}$ is a force acting on the contact area of elastic impacts between the particles i and j. $\mathbf{T}_{i,contact}$ is the summation of torques caused by the contact forces between particles

$$\mathbf{T}_{i,contact} = \sum_{j=1, j \neq i}^{N} \mathbf{T}_{ij} = \sum_{j=1, j \neq i}^{N} \mathbf{d}_{ij} \times \mathbf{F}_{ij} \tag{6}$$

where $\mathbf{d}_{cij}$ is the vector pointing from the centre of gravity of particle i to the contact point with particle j.

The particles of a granular material were of the same material. The simplest linear elastic repulsion and dissipation forces model for normal inter-particle contact forces between two particles i and j was applied.

$$\mathbf{F}_{n,ij} = \mathbf{F}_{n,ij,elastic} + \mathbf{F}_{n,ij,viscous} \tag{7}$$

10

$$\mathbf{F}_{n,ij,elastic} = k_n R_{ij} h_{ij} \mathbf{n}_{ij} \tag{8}$$

$$\mathbf{F}_{n,ij,viscous} = -\gamma_n m_{ij} \mathbf{v}_{n,ij} \tag{9}$$

where k_n is the spring stiffness coefficient related to Young's modulus, γ_n is the normal dissipation coefficient and m_{ij} is the reduced mass of the contacting particles i and j

$$m_{ij} = \frac{m_i m_j}{m_i + m_j} \tag{10}$$

R_{ij} is the equivalent radius

$$R_{ij} = \frac{R_i R_j}{R_i + R_j} \tag{11}$$

of particles in contact with the radii R_i and R_j, and h_{ij} is the depth of contact overlap.

The tangential force acting between particles was expressed by the Coulomb criteria

$$\mathbf{F}_{t,ij} = -\mathbf{t}_{ij} \min \left(\gamma_t m_{ij} |\mathbf{v}_{t,ij}|, \mu |\mathbf{F}_{n,ij}| \right) \tag{12}$$

with γ_t being the tangential dissipation coefficient and μ closely related to the dynamic friction coefficient.

The solution of the equations (1), (2), (3) and (4) is obtained by a 5th order *Gear predictor-corrector* scheme. The time step Δt of the integration was chosen such that the entire contact between the particles would be resolved at least within 10 time steps.

The boundary conditions are defined by walls, which were defined as particles too and were of the same material. Contact forces acting between particles and walls are defined in the same way as between particles.

The simulation method was programmed in the programming language C++ (Stroustrup (1991)) by using OOP methodology (Peters and Džiugys (1998), and Peters and Džiugys (1998b)). This approach supports objects that describes various dimensions, shapes and sizes for particles as well as for the walls as boundaries of simulation area. The description of motion dynamics of particles is universal for all shapes and is defined at the first stages of the abstraction. The programming code is implemented in the TOSCA (Tools of Object-oriented Software for Continuum mechanic Applications) software package, which allows for a high degree of flexibility and for the shortening the software development process (Peters (1996) and Peters (1997)).

3 Contact Detection Algorithm for Ellipses

3.1 Introduction

Ellipses for two-dimensional particles and ellipsoids for three-dimensional particles are other often used shapes, because various kinds of granular material particle resemble these shapes. Therefore, according to Rothenburg and Bathurst (1991) the characteristics of granular material are better represented by systems of ellipsoidal particles than by systems of spherical particles. For discussions of the implementation of ellipses and ellipsoids, see Lin and Ng (1995), Lin and Ng (1997).

At this time, various analytical methods of contact detection for two- and three- dimensional elliptical particles are constructed by intersection, geometric potential and common normal algorithms.
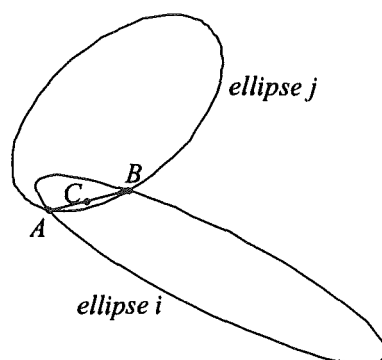
Figure 3: Contact of two ellipses according to intersection algorithm

Two similar *intersection* algorithms developed by Rothenburg and Bathurst (1991) and Ting (1991) are based on idea to find contact location, point C, as the midpoint of the line joining the intersection points A and B (Fig. 3). Location of the points A and B is the result of solution of quartic polynomial equation, which may be solved analytically or iteratively. However, this method has difficulties with accuracy and stability. When overlap area is very small or even a point (what is often for stiff particles), or when semi-axes of ellipses are aligned each with other, the resulting quartic equation can be ill conditioned. More discussions about that problem could be found

12

in Ting (1992) and Ting *et al.* (1993). Another problem is that this method is not straightforward extendible into three-dimensional particles.
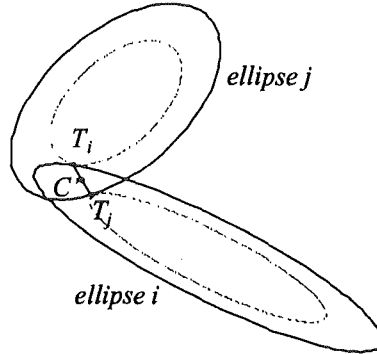
Figure 4: Contact of two ellipses according to geometric potential algorithm

Alternatively, Ting (1992) and Ng (1992) developed two basically similar *geometric potential* algorithms where contact location, point C', is defined as the midpoint of the line joining the "touch" points T_i and T_j (Fig. 4). The point T_i is defined as a "deepest" point of ellipse i inside ellipse j, and the point T_j - as a "deepest" point of ellipse j inside ellipse i. The algorithm developed by Ting results a quartic polynomial equation, which is better conditioned as one, obtained by intersection algorithm (Ting (1992)). Trigonometric equation obtained by Ng is equivalent to quartic polynomial of Ting what means that both algorithms have the same stability and accuracy. Besides, Lin and Ng (1995) developed more common geometric potential algorithm for three-dimensional particles.

Lin and Ng (1995) described *common normal* algorithm (Fig. 5) developed for two- and three-dimensional particles. After testing, they concluded that algorithm based on geometric potential was more favourable in terms of accuracy and efficiency and was used for later simulations in Lin and Ng (1997).

As result, analytical solutions of contact detection for two-dimensional elliptical particles requires the solution of a 4th polynomial (e.g. Rothenburg and Bathurst (1991) and Ting (1992)). This can be done by an analytical or an numerical methods. However, both methods have to detect and to determine an overlap accurately, in particular for usually small regions of

13
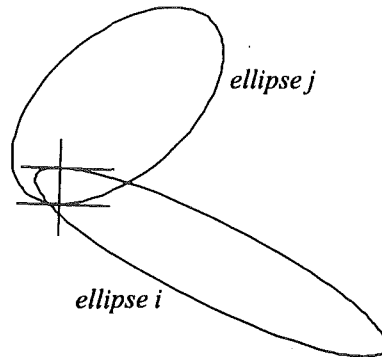
Figure 5: Contact of two ellipses according to the common normal concept

contact. Today existing *intersection* (Rothenburg and Bathurst (1991) and Ting (1991)) and *geometric potential* (Ting (1992)) algorithms results to the 4th polynomial which can be ill-conditioned when overlap area is very small or even a point (what is often for stiff particles), or when semi-axes of ellipses are aligned each with other, what gives unstable solution of ellipse shapes overlap.

Below, we describe a new algorithm to calculate contact overlap of two-dimensional ellipses which appeared to be more stable than one of Ting (1992).

14

3.2 Description of the Algorithm

Let two elliptical particles i and j, which shapes are defined by parameters $\{x_i, y_i, a_i, b_i, \theta_j\}$ and $\{x_j, y_j, a_j, b_j, \theta_j\}$ in contact. (Fig. 6)
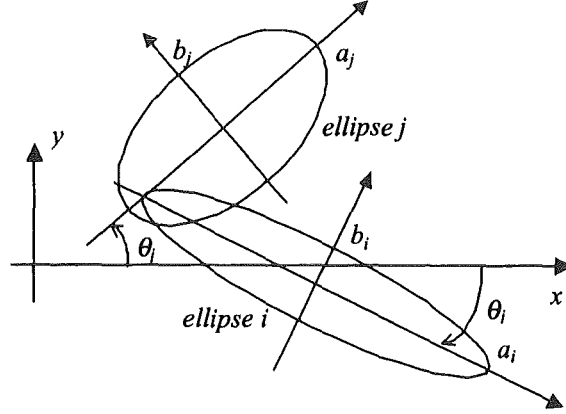
Figure 6: Initial position of two ellipses in contact

Thus, the shapes of the ellipses i and j are described by equations

$$
\begin{aligned}
f_i(x,y) &= A_i (x-x_i)^2 + B_i (y - y_i)^2 + 2C_i (x - x_i)(y - y_i) - 1 = 0 \quad (13) \\
f_j(x,y) &= A_j (x-x_j)^2 + B_j (y - y_j)^2 + 2C_j (x - x_j)(y - y_j) - 1 = 0
\end{aligned}
$$

where coefficients A, B ad C are defined as

$$
A = \left(\frac{\cos\theta}{a}\right)^2 + \left(\frac{\sin\theta}{b}\right)^2 \qquad (14)
$$

$$
B = \left(\frac{\sin\theta}{a}\right)^2 + \left(\frac{\cos\theta}{b}\right)^2
$$

$$
C = \cos\theta \sin\theta \left(\frac{1}{a^2} - \frac{1}{b^2}\right)
$$

$\{x, y\}$ is location of ellipse centre in world frame reference, a and b are semi-axes and θ is the angle between the major semi-axis of the ellipse and the x-axis of the Cartesian co-ordinate system. In order to calculate "touch" points T_i and T_j and the overlap a sequence of three transformations of co-ordinates is carried out to transfer ellipses into a more convenient form.

15
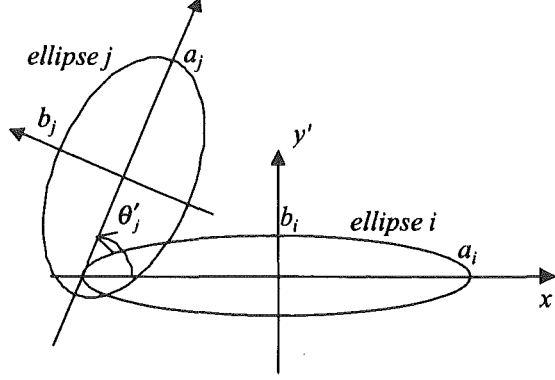
Figure 7: Two ellipses in contact in co-ordinate system $\{x',y'\}$

The first co-ordinate transformation $\{x,y\} \rightarrow \{x',y'\}$

$$x' = (x - x_i)\cos\theta_i + (y - y_i)\sin\theta_i \tag{15}$$
$$y' = -(x - x_i)\sin\theta_i + (y - y_i)\cos\theta_i$$

sets ellipse i into canonical form with the centre of ellipse i in the origin of frame reference $\{x',y'\}$ and the semi-axes parallel to the axes of co-ordinates (Fig. 7)

$$f_i(x',y') = \left(\frac{x'}{a_i}\right)^2 + \left(\frac{y'}{b_i}\right)^2 - 1 = 0 \tag{16}$$

Then ellipse j is described as

$$f_j(x',y') = A'_j\left(x' - x'_j\right)^2 + B'_j\left(y' - y'_j\right)^2 + 2C'_j\left(x' - x'_j\right)\left(y' - y'_j\right) - 1 = 0 \tag{17}$$

where coefficients of ellipse j are defined as follows

$$A'_j = \left(\frac{\cos\theta'_j}{a_j}\right)^2 + \left(\frac{\sin\theta'_j}{b_j}\right)^2 \tag{18}$$

$$B'_j = \left(\frac{\sin\theta'_j}{a_j}\right)^2 + \left(\frac{\cos\theta'_j}{b_j}\right)^2$$

$$C'_j = \cos\theta'_j\sin\theta'_j\left(\frac{1}{a_j^2} - \frac{1}{b_j^2}\right)$$

16

where

$$\theta'_j = \theta_j - \theta_i, \tag{19}$$
$$x'_i = 0, y'_i = 0$$

$$x'_j = (x_j - x_i)\cos\theta_i + (y_j - y_i)\sin\theta_i \tag{20}$$
$$y'_j = -(x_j - x_i)\sin\theta_i + (y_j - y_i)\cos\theta_i$$

The second co-ordinate transformation $\{x', y'\} \rightarrow \{X', Y'\}$

$$X' = \frac{x'}{a_i} \tag{21}$$

$$Y' = \frac{y'}{b_i}$$

will transform ellipse i into a circle with radius equal to 1 and its centre positioned in the origin of frame reference $\{X', Y'\}$ (Fig. 8)
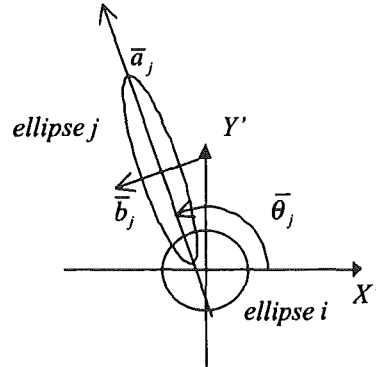
Figure 8: Two ellipses in contact in co-ordinate system $\{X', Y'\}$

$$f_i(X', Y') = X'^2 + Y'^2 - 1 = 0 \tag{22}$$

This furthers the following description of ellipse j

$$f_j(X', Y') = \bar{A}_j \left(X' - X'_j\right)^2 + \bar{B}\left(Y' - Y'_j\right)^2 + 2\bar{C}\left(X' - X'_j\right)\left(Y' - Y'_j\right) - 1 = 0 \tag{23}$$

17

where

$$\bar{A}_j = a_i^2 A_j' \tag{24}$$
$$\bar{B}_j = b_i^2 B_j'$$
$$\bar{C}_j = a_i b_i C_j'$$

$$X_j' = \frac{x_j'}{a_i} \tag{25}$$

$$Y_j' = \frac{y_j'}{b_i}$$

Parameters $\bar{a}_j$, $\bar{b}_j$ and $\bar{\theta}_j$ of the ellipse j in frame reference $\{X', Y'\}$ may be calculated by

$$\bar{a}_j = \sqrt{\frac{2}{\bar{A}_j + \bar{B}_j + \frac{\bar{A}_j - \bar{B}_j}{\cos\left(2\bar{\theta}_j\right)}}} \tag{26}$$

$$\bar{b}_j = \sqrt{\frac{1}{\bar{A}_j + \bar{B}_j - \frac{1}{\bar{a}_j^2}}} \tag{27}$$

$$\bar{\theta}_j = \frac{1}{2} arctg \left(\frac{-2\bar{C}_j}{-\left(\bar{A}_j - \bar{B}_j\right)} \right) \tag{28}$$

The third co-ordinate transformation $\{X', Y'\} \rightarrow \{X, Y\}$

$$X = \left(X' - X_j'\right) \cos\bar{\theta}_j + \left(Y' - Y_j'\right) \sin\bar{\theta}_j \tag{29}$$
$$Y = -\left(X' - X_j'\right) \sin\bar{\theta}_j + \left(Y' - Y_j'\right) \cos\bar{\theta}_j$$

transforms the centre of ellipse j into the origin of frame reference $\{X, Y\}$ and the centre of ellipse i in the position $O_i(X_i, Y_i)$ (Fig. 9)

$$X_i = -X_j' \cos\bar{\theta}_j - Y_j' \sin\bar{\theta}_j \tag{30}$$
$$Y_i = X_j' \sin\bar{\theta}_j - Y_j' \cos\bar{\theta}_j$$

This yields the final form of the equations for the ellipses i and j:

$$f_i(X, Y) = (X - X_i)^2 + (Y - Y_i)^2 - 1 = 0 \tag{31}$$

18

$$f_j(X,Y) = \left(\frac{X}{\bar{a}_j}\right)^2 + \left(\frac{Y}{\bar{b}_j}\right)^2 - 1 = 0 \tag{32}$$

If a circle with radius ρ_T is defined, which shares the origin together with circle (ellipse) i in the point O_i, and touches the ellipse j in the point T_j (X_{Tj}, Y_{Tj}) (Fig. 9), then point T_j is the nearest point of ellipse j to the point O_i. At the same time, the point T_j is the same "touch" point defined in geometric potential algorithms of Ting (1992) and Ng (1992) (Fig. 4).

Let us define ρ as the distance from O_i to any point of ellipse j as follows

$$\rho^2 = (X - X_i)^2 + (Y - Y_i)^2 \tag{33}$$

After substituting Y expressed from (32) into equation (33)

$$\rho^2 = (X - X_i)^2 + \left(\pm k\sqrt{\bar{a}_j^2 - X^2} - Y_i\right)^2 \tag{34}$$

where $k = \bar{b}_j/\bar{a}_j \leq 1$.

Now, the location of the point T_j may be found analytically or iteratively by determining the shortest distance

$$\rho_T = \min(\rho) \tag{35}$$

If ellipses are overlapping then point T_j is inside circle i, $i.e.$ the distance ρ_T from point O_i (X_i, Y_i) to the point T_j (X_{Tj}, Y_{Tj}) must satisfy the condition

$$\rho_T = \sqrt{(X_{Tj} - X_i)^2 + (Y_{Tj} - Y_i)^2} \leq 1 \tag{36}$$

otherwise there is no overlap.

The position of the "touch" point T_j now can be calculated analytically or iteratively from the equation (34) according to the conditions (35) and (36). Below we present an analytical solution.
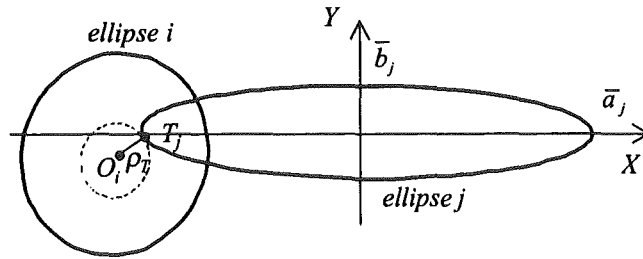
Figure 9: Two ellipses in contact in co-ordinate system $\{X, Y\}$

19

3.2.1 Analytical Solution

According to the condition (35), the location of the "touch" point T_j as the nearest point of the ellipse j from the origin of circle (ellipse) i may be calculated by the differential equation

$$\frac{\partial \rho^2}{\partial X} = 0 \tag{37}$$

Substitution of (34) into (37) and differentiation gives a quartic polynomial

$$a_1 X^4 + a_2 X^3 + a_3 X^2 + a_4 X + a_5 = 0 \tag{38}$$

where

$$
\begin{aligned}
a_1 &= \left(1 - k^2\right)^2 \\
a_2 &= -2\left(1 - k^2\right) X_i \\
a_3 &= Y_i^2 k^2 + X_i^2 - \bar{a}_j^2 \left(1 - k^2\right)^2 \\
a_4 &= 2\bar{a}_j^2 \left(1 - k^2\right) X_i \\
a_5 &= -X_i^2 \bar{a}_j^2
\end{aligned}
\tag{39}
$$

The solution of equation (38) gives a set of four complex roots $X_l, l = [1,4]$. Only real roots of the set of $X_l (Im(X_l) = 0)$ are used to calculate Y from (32). The resulting set of (X, Y) under applying the condition (35) gives the location of the point $T_j(X_{Tj}, Y_{Tj})$.

Ellipse i overlaps with ellipse j if the location of T_j satisfies the condition (36). Finally, the co-ordinates of "touch" point $T_j(x_{Tj}, y_{Tj})$ in the laboratory frame reference $\{x, y\}$ are restored by a sequence of reverse transformations of co-ordinates. Another "touch" point T_i on the ellipse i is calculated by the same algorithm.

Due to limited computer accuracy, calculation of analytical solution of polynomial (38) is complicated only for $k = \bar{b}_j / \bar{a}_j \rightarrow 1$ or $X_i \rightarrow 0$. But then, location of T_j may be found simply without solution of quartic polynomial (38) in these cases. Therefore present algorithm appeared to be more reliable than Ting (1992) algorithm, which may result ill-conditioned quartic polynomial in other cases of ellipses parameters.

Solution of the quartic polynomial (24) may be non-stabile (unreliable) due to considerable round-off errors which may be caused by limited computer accuracy. Below the analysis of such possibilities is presented.

20

By substitution of

$$X = z + \frac{X_i}{2\left(1 - k^2\right)} \qquad (40)$$

the quartic polynomial (38) is transformed into non-full quartic polynomial

$$z^4 + pz^2 + qz + r = 0 \qquad (41)$$

where parameters p, q and r are defined as

$$p = \frac{2Y_i^2 k^2 - X_i^2 - 2\bar{a}_j^2\left(1 - k^2\right)^2}{2\left(1 - k^2\right)^2} \qquad (42)$$

$$q = X_i \frac{Y_i^2 k^2 + \bar{a}_j^2\left(1 - k^2\right)^2}{\left(1 - k^2\right)^3} \qquad (43)$$

$$r = X_i^2 \frac{4Y_i^2 k^2 + X_i^2 - 4\bar{a}_j^2\left(1 - k^2\right)^2}{16\left(1 - k^2\right)^4} \qquad (44)$$

The polynomial (41) is solved by standard analytical procedure (Korn and Korn (1968)) through roots of the cubic polynomial

$$w^3 + \frac{p}{2}w^2 + \frac{p^2 - 4r}{16}w - \frac{q}{64} = 0 \qquad (45)$$

Roots of (41) is calculated as

$$z = \pm\sqrt{w_1} \pm \sqrt{w_2} \pm \sqrt{w_3} \qquad (46)$$

where signs are selected by the condition

$$\left(\pm\sqrt{w_1}\right) \cdot \left(\pm\sqrt{w_2}\right) \cdot \left(\pm\sqrt{w_3}\right) = -\frac{q}{8} \qquad (47)$$

But due to limited computer accuracy, solution of the polynomial (41) is complicated and unstable at least in two cases.

The first trouble case is when $k = \bar{b}_j / \bar{a}_j$ approaches to one, because it leads to considerable round-off errors. But in this case ellipse j may be treated as circle in frame reference $\{X, Y\}$ and T_j may be calculated by simpler algorithm without problem.

The second trouble case is when parameter q approaches to zero. Due to round-off errors the choosing procedure of roots by the condition (47)

21

may be unreliable. In the present algorithm, it may happen when $X_i \to 0$. The procedures of solution of T_j are trivial in these cases and may be found without solution of quartic polynomial (38).

Result of Ting (1992) geometric potential algorithm parameter is quartic polynomial too. And parameter q of non-full quartic polynomial of Ting (1992) may approach to zero in some other cases. Such example is for ellipses defined as $x_i = 0.0490546$, $y_i = 0.0826842$, $a_i = 0.00427403$, $b_i = 0.00347603$, $t_i = 1.66736$, $x_j = 0.0554617$, $y_j = 0.0797356$, $a_j = 0.00430882$, $b_j = 0.00247172$, $t_j = 2.24469$ (Fig. 10), which results to $q = -2.09 \cdot 10^{-5}$. As a way out is to consider the quartic polynomial (41) as a quadratic polynomial by $q = 0$ and the substitution of $Z = z^2$, i.e.

$$Z^2 + pZ + r = 0 \tag{48}$$

But in certain locations of ellipses, it may result to no real roots at all for equation (38), if discriminate of the quadratic equation (48) is negative (for the example $discriminate = 1.35817 \cdot 10^{-6}$). So solution may be unstable.
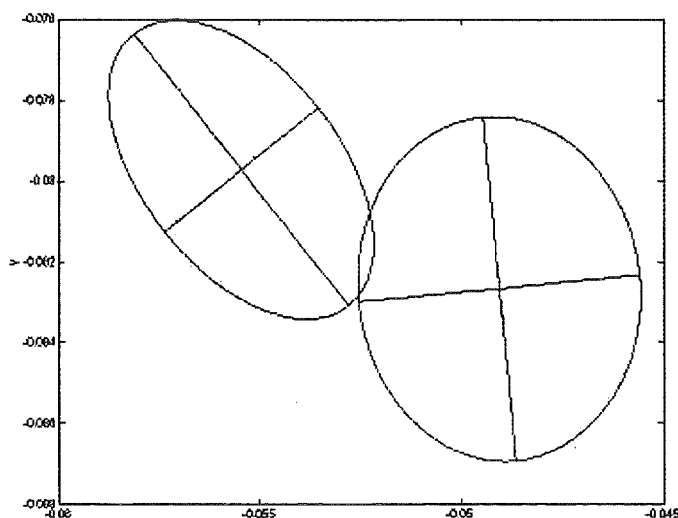
Figure 10: An example of two ellipses contact

22

3.2.2 Iterative Solution
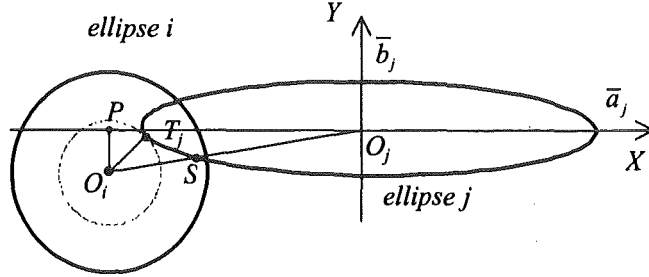
Figure 11: The limits for searching the location of the touch point T_j

Too many methods exist to find iteratively the touch point $T_j(X_{Tj}, Y_{Tj})$ by looking for the shortest distance from the point O_i - origin of the ellipse i to the ellipse j according to the equation (34) and the condition (35).

The main problem is to optimise method by narrowing the limits for the searching of possible location of the touch point T_j.

The touch point T_j is located within the semi-plane bounded by lines through the centres of both ellipses and furthermore is inside the triangle which is defined by three points $O_i(X_i, Y_i)$, $O_j(X_j = 0, Y_j = 0)$ and $P(X_i, 0)$ (Fig. 11). This defines three conditions to determine the position of the touch point.

The first condition is that T_j is located in the same quarter of frame reference as O_i

$$sign\,(X_{Tj}) = sign\,(X_i)$$
$$sign\,(Y_{Tj}) = sign\,(Y_i) \tag{49}$$

The second condition is that

$$|X_{Tj}| \leq \min\,(|X_i|, \bar{a}_j) \tag{50}$$

The last condition defines that T_j is on the ellipse j between the crossing point S of the line, connecting the origins of the ellipses O_i and O_j, and the X-axis.

$$|X_{Tj}| \geq \frac{|X_i|}{\sqrt{\left(\frac{X_i}{a_j}\right)^2 + \left(\frac{Y_i}{b_j}\right)^2}} \tag{51}$$

23

$$|Y_{Tj}| \geq \frac{|Y_i|}{\sqrt{\left(\frac{X_i}{a_j}\right)^2 + \left(\frac{Y_i}{b_j}\right)^2}} \qquad (52)$$

24

4 Simulation results

4.1 Motion of Spheres in a Rectangular Enclosure

The possibilities offered by the method to simulate particle motion in general and on a moving grate or in a rotary kiln of a combustion device in particular are demonstrated for the two-dimensional motion of granular material consisting of 500 three-dimensional spherical of different sizes but of the same material properties, of which the relevant details are listed in Table 1.

Since the initial conditions for particles moving or resting in a packed bed cannot be specified a priori, the calculations were carried out in two stages. Especially since the packaging of the particles results from their previous dynamics, plausible initial conditions can only be obtained by a separate calculation. The first calculation was started with the setup shown in Fig. 12.

Initially, the three-dimensional particles were distributed on an orthogonal and uniform grid represented by a two-dimensional box of $2 \times 3\,\mathrm{m}$ in size (Fig. 12). The size of the grid cells was equal to the diameter of the largest particle. Thus, particles placed in the centre of the cells did not experience contact with their neighbours. Particle size and initial velocities of the individual particles were chosen randomly. The components of the velocity and the position into the y-direction were set to zero, which limits the motion to the xz-plane. The subsequent motion of particles was calculated taking into account the influence of gravity forces ($g_x = -10\,\mathrm{m}/\mathrm{s}^2, g_y = g_z = 0$) and particle contacts occurring during motion. The final result shows how the particles came to rest within a particular arrangement (Fig. 13).

The random distribution of particles and void space determines the total volume needed for the arrangement. The grey-coloured scale of the particles represents the overall contact forces acting on a particle

$$f_i = \sum_{j \neq i} |\mathbf{F}_{ij}| \qquad (53)$$

which are inhomogeneously distributed in the packed bed. Connections between neighbouring particles with approximately the same load display the typical arc structures of such arrangements. These arcs act as bridge-like structures concentrating loads on a few particles at the base of their "pillars" and thus hinder the motion.

The results obtained from these calculations were taken as initial conditions for the following calculation, which predicts the motion of particles

Particle radius	R	0.03 - 0.05 m
Initial velocity	v	0 - 1 m/s
Density	ρ	1000 kg/m^3
Normal spring stiffness coefficient	k_n	5.0·10^5 Pa
Normal energy dissipation coefficient	γ_n	100 s^{-1}
Tangential energy dissipation coefficient	γ_t	20 s^{-1}
Friction coefficient	μ	100

Table 1: Spherical particle data
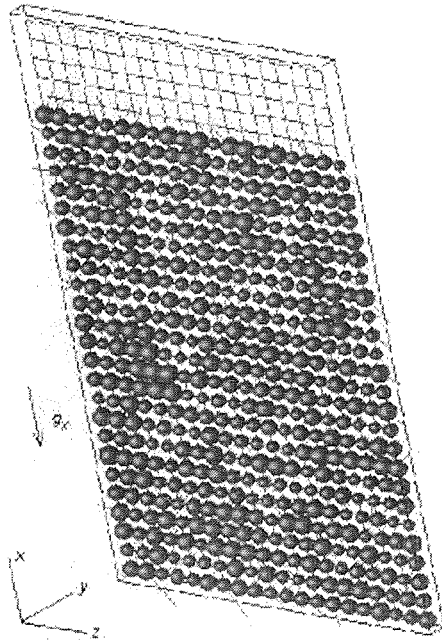
Figure 12: Setup for particle motion: 2D problem in pseudo 3D plane
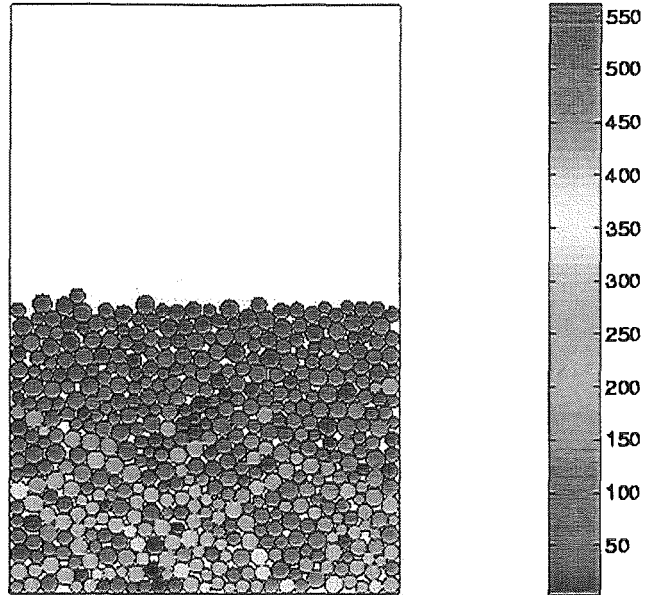
Figure 13: Particles at rest
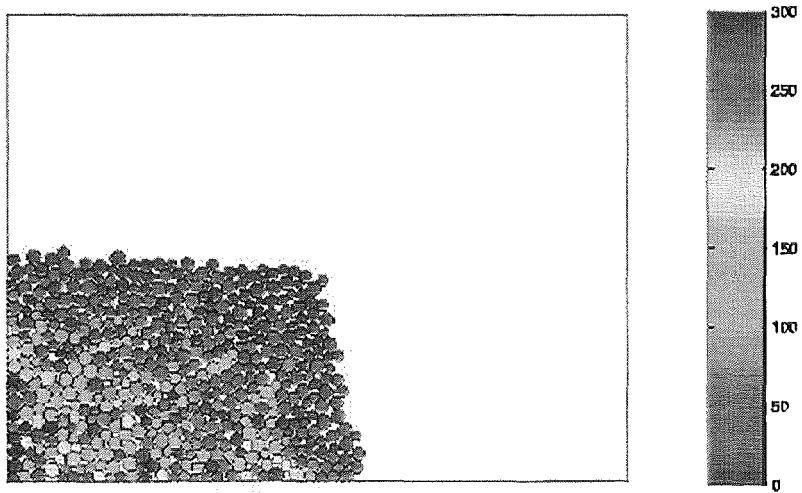
Figure 14: Start of discharge of particles
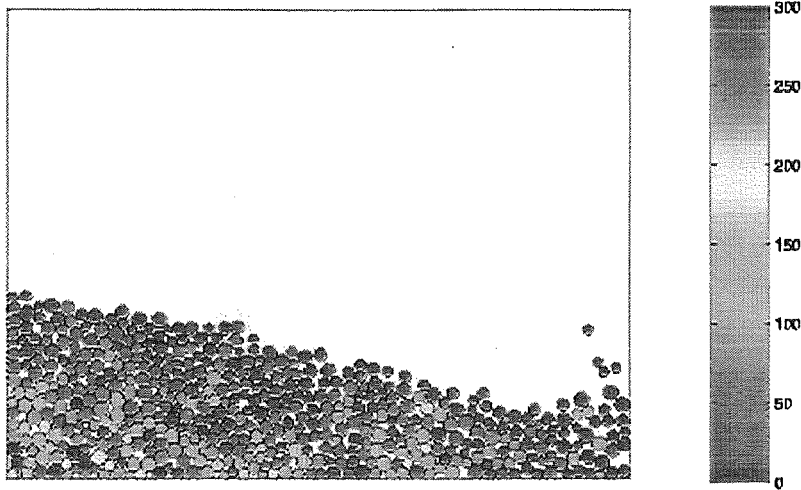
Figure 15: Discharge of particles into a combustion chamber

when they are discharged through an open gate into a combustion chamber of 4 × 3 m in size. In order to simulate this behaviour, the right wall of the box in Fig. 13 was displaced by a certain distance at the start of the calculation. A front of moving particles penetrates the open space like an avalanche as shown in Fig. 14.

Once the gate opens, the particles accumulated just behind it discharge into the combustion chamber, moving freely under the effect of gravity forces. While a liquid is subject to the linear variation of the pressure as a function of the depth, the moving bed experiences an inhomogeneous load distribution during the entire motion. During the motion of the bed, the particles order themselves into structures with the contact between them in the bed being more or less strong. These structures are shown in Fig. 14 and Fig. 15 and indicated by the different colours. If particles experiencing approximately the same load were connected by imaginary lines, these would delimit the structures. They extend throughout the bed and in some cases reaching its upper surface. Fig. 15 displays the state of the calculation when the front reaches the opposite wall, from where the particles bounce back, some of them leaving the formation completely.

In general, particles in this region have a very loose contact with their neighbours, resembling a fluidised bed to a certain extent. As a result, the

void space has increased as compared to a packed arrangement. Again, branches of tree-like structures for the distribution of particles with approximately the same load become apparent and remain throughout the entire motion.

4.2 Motion of Spheres in a Rotary kiln

The following example depicts the mixing of granular material in a rotary kiln. Initially, the three-dimensional spherical particles were randomly distributed on a two-dimensional grid inside drum of 1.5 m radius, in similar way to the case of the previous chapter. Under the influence of gravity the particles came to rest after 2 seconds and then the drum started to rotate with an angular velocity $w_y = 1\,\mathrm{s}^{-1}$.

Avalanches occurring during the mixing process form rather flat surfaces of granular material (Fig. 16). However, the flow of particles may also form wave-like irregularities on the surface of the granular material (Fig. 17), which depend on the inner structure of the granular material and distribution of the contact force.
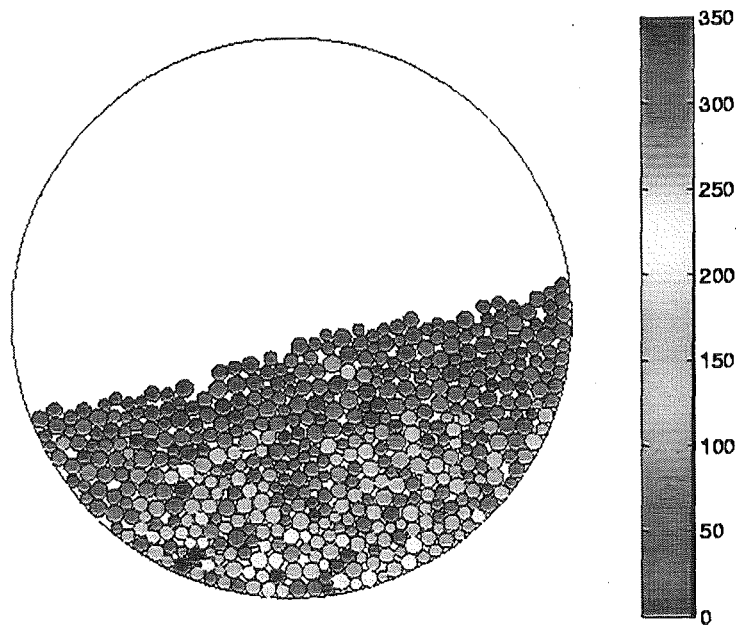
Figure 16: Particles in rotary kiln - almost flat surface of the granular material
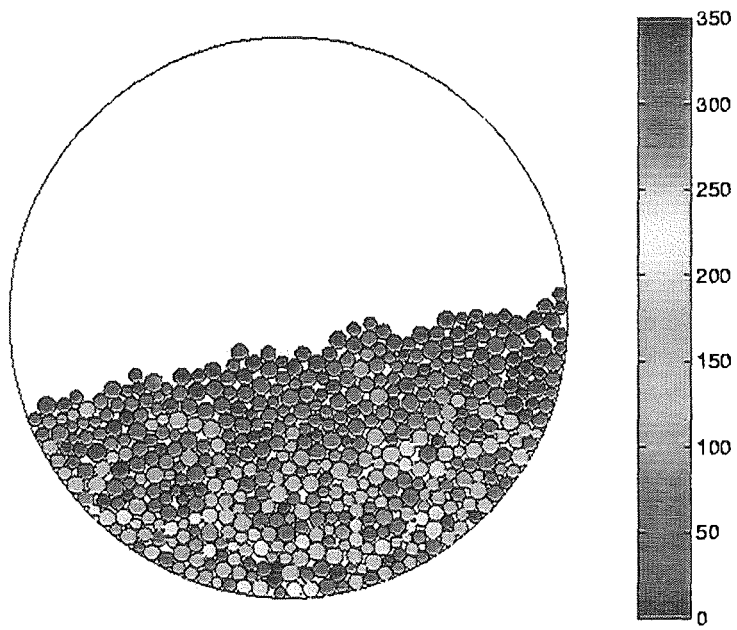
Figure 17: Particles in rotary kiln - waves on the surface of the granular material

4.3 Motion of Ellipses in a Rotary kiln

Material properties, employed for the current simulation in a rotary kiln are listed in Table 2.

Initial conditions were specified similar to the case of the previous chapter. Fig.18 shows an image of the particles falling under the influence of gravity and inter particle contacts.

At an initial stage, particles almost do not experience any contacts with each other, so that they move freely under the influence of gravity and initial velocity. The motion is bounded by the bordering shape of the rotary kiln, which firstly stops the purely vertical motion and secondly causes particle to interact with each other as shown in Fig.18 for a time of $t = 0.1$ s.

Approximately half of the particles still fall down without contact to their neighbours, while a denser arrangement with increasing particle interaction takes place in the bottom part of the rotary kiln. Here, particles already experience several contact with their neighbours, indicated by the colour scale for the allover forces acting on a particle. Finally, all particles come to rest packed in the bottom part of the rotary kiln. At this stage, the random distribution of particles and void space determine the total volume needed for the arrangement.

The following Figs. 19, 20 and 21 depict the arrangement of particles during the transition of mainly vertical motion during the packaging process to rotational motion at time steps of $t = 1, 1.5, 2$ s.

While a liquid is subject to the linear variation of pressure as a function of the depth, the moving bed experiences an inhomogeneous load distribution during entire motion. During the motion of the bed, the particles order themselves into structures with the contact between them in the bed being more or less strong. The colour scale of the particles represents the overall contact forces acting on a particle. Fig. 19 and 20 show rather inhomogeneous load patterns of the particles. While in Fig. 20 medium forces of approximately $f = 10 - 12$ N govern the load in the bottom part of the kiln, the load distribution in Fig. 19 displays a smaller load level of approximately $f = 6$ N in this region.

Fig. 21 depicts the typical arc structures of such arrangements, which are build up of particles connected by approximately the same load.

If particles experiencing approximately the same load were connected by imaginary lines, these would delimit these structures. These arcs act as bridge-like structures concentrating loads on a few particles at the base of

Particle Semi-axis	R	0.001 - 0.005 m
Initial velocity	v	0 - 1 m/s
Density	ρ	1000 kg/m^3
Elastic constant	C	10^8 Pa
Normal spring stiffness coefficient	k_n	5.0·10^5 Pa
Normal energy dissipation coefficient	γ_n	100 s^{-1}
Tangential energy dissipation coefficient	γ_t	20 s^{-1}
Friction coefficient	μ	0.6

Table 2: Elliptical particle data

their "pillars" and, thus, hinder the motion.

Furthermore, the velocity vectors and its direction in Fig. 22, attached to the centre of particles, show the motion of the centre of gravity of each particle. The velocity vectors indicate an inner and an outer loop, which the particles follow. The inner and outer loop represent a segregation of small and large particles, whereby smaller particles gather in the centre surrounded by bigger particles. The inner loop is located at approximately the centre of the packed bed, whereas particles of the outer loop follow the path along the surface of the packed bed and the contour of the rotary kiln. This effect is caused by different potential and kinetic energy of particles emerging on the right hand side of the surface of the packed bed. Large particles, sliding down the slope of the packed bed reach the lower end of the slope due to a higher kinetic energy, while smaller particles already come to rest halfway the slope. There, they separate from bigger particles and enter the inner loop.
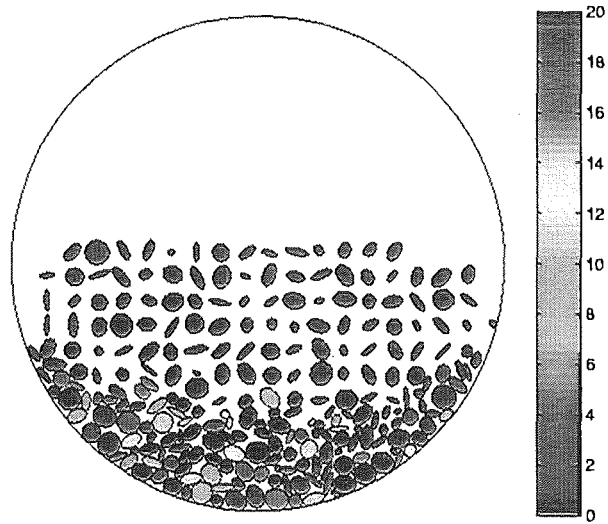
Figure 18: Motion in a rotary kiln and distribution of particle forces [N], $t = 0.1$ s
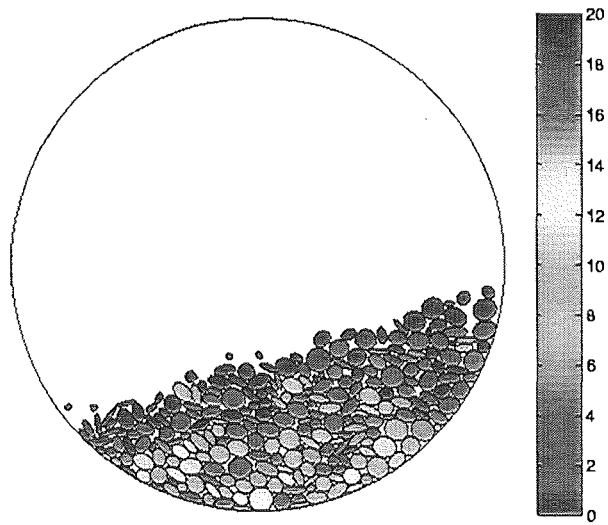
Figure 19: Motion in a rotary kiln and distribution of particle forces [N], $t = 1$ s
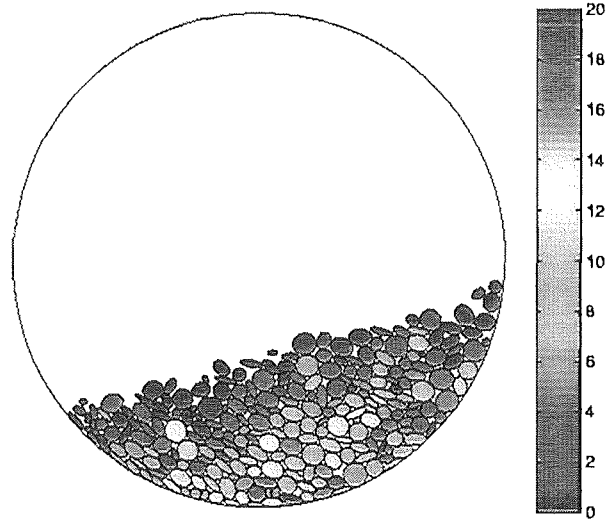
Figure 20: Motion in a rotary kiln and distribution of particle forces [N],
$t = 1.5$ s
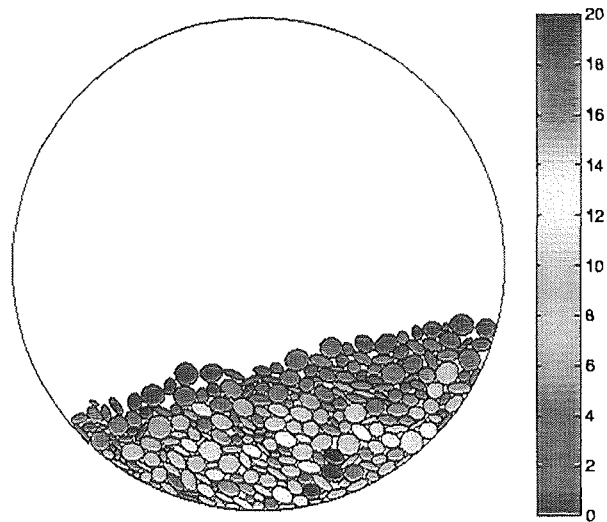
Figure 21: Motion in a rotary kiln and distribution of particle forces [N],
$t = 2$ s

35
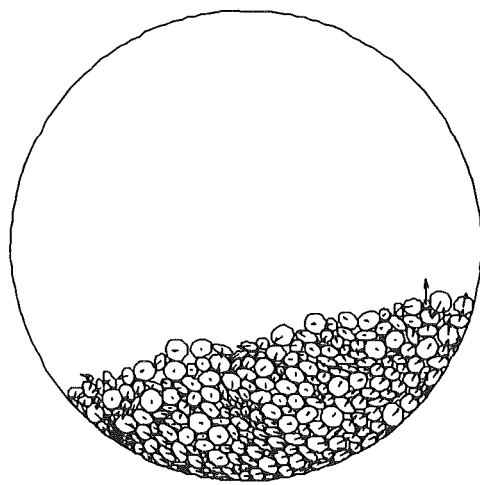
Figure 22: Motion in a rotary kiln and distribution of particle velocities, $t = 2$ s

4.4 Motion on a Travelling Grate

The following Fig. 23 depicts the instantaneous distribution of particle positions and velocities for the transport on a travelling grate.
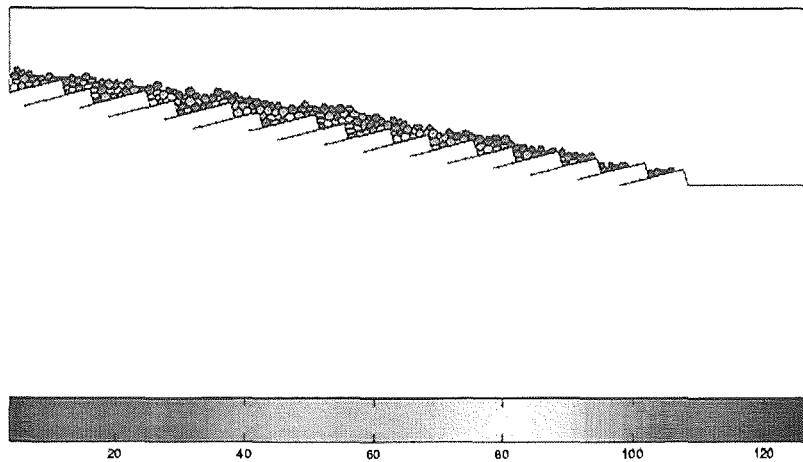
Figure 23: Motion on a moving grate and distribution of particle forces [N]

A part of the grate with its particles extracted is depicted in Fig. 24 to show particle velocities. A maximum value of the velocity of $v = 0.09\,\mathrm{m/s}$ occurs due to the kinetics of the grate. Although, the motion of the particles is inhomogeneous, a major direction of the motion along the grate dominates. This indicates, that only little lateral e.g. versus the bed height occurs, and thus, the bed motion resembles a rigid body motion to a large extent Hunsinger et al. (2000) and Beckmann and Scholz (2000).

In general the load of particles increases with depth of the bed. However, arc-like structures, caused by the arrangement and the contact of particles, may prevent high loads on particles located on the grate surface.
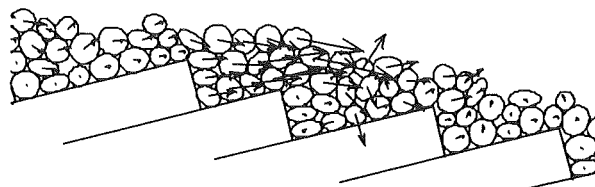
Figure 24: Motion on a moving grate and distribution of particle velocities

4.5 Three-dimensional Packing of Soot Particles on a Filter

The last application deals with the arrangement of spherical particles on a filter to demonstrate the capabilities of the method for the predictions of 3-dimensional motion of particles. Filters for separation of solid particles are often used in technical applications and the packing of the particles on the filter surface is of particular interest. The latter is characterised by the porosity of the filtered particulate phase and allows to estimate loading and regeneration of the filter versus time. Therefore, the simulation method was applied to investigate the packing of spherical soot particles on a filter surface. The size distribution was taken from experimental measurements and is shown in the following Fig. 25 and Table 3.
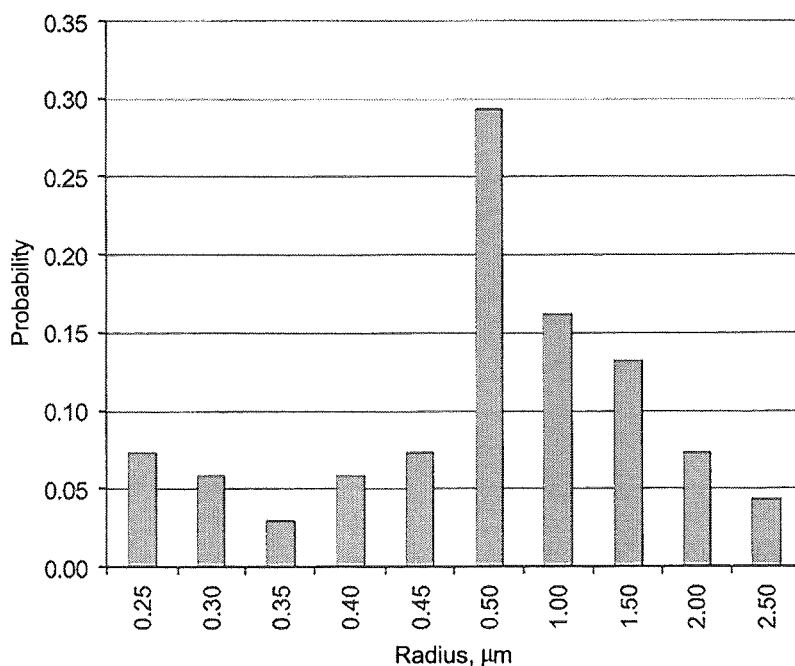
Figure 25: Distribution of the soot particles size

particle radius, μm	0.25	0.3	0.35	0.4	0.45
probability	0.074	0.059	0.029	0.059	0.074
particle radius, μm	0.5	1	1.5	2	2.5
probability	0.294	0.162	0.132	0.074	0.044

Table 3: Distribution of sizes of soot particles

The sizes of the particles were chosen according to the given distribution, whereas the initial velocity of individual particles was assigned randomly up to a maximum value of $v_{max} = 0.5$ mm / s. The initial positions of the particles were specified above the filter, from were the soot particles fall under the influence of gravity onto the filter surface. The following Fig. 26 depicts an intermediate stage during the packing of the soot particles.
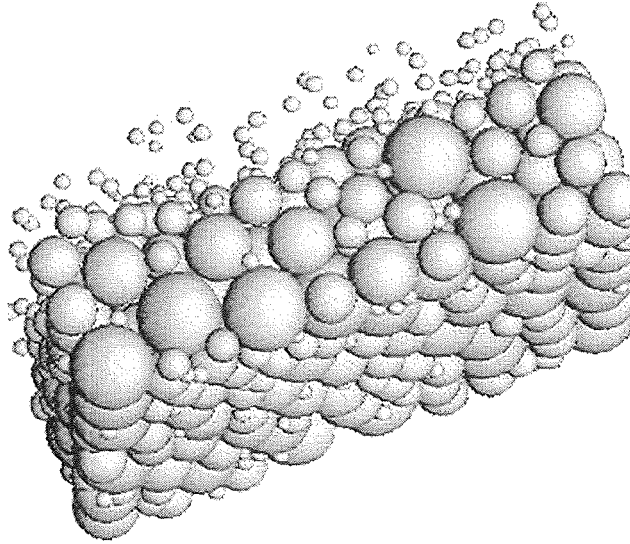
Figure 26: Packing of soot particles on the filter

The distribution is mainly governed by the largest particles and some of the void space between the particles is occupied by smaller particles, which amounts to a value of the porosity of $e \sim 43\%$.

5 Summary

Within this study a simulation method for the motion of granular material
was approved to be applicable for the motion of fuel particles in combustion
devices. The latter include different means of transport such as motion on
a travelling grate or in a rotary kiln. The variety of geometrical forms of
the fuel particles requires an additional elliptical shape beside a spherical
shape. For the latter no difficulties arise to detect the overlap, however, to
determine the contact for elliptical particles involved the development of a
new algorithm. It is based on a sequence of transformations and thus, reduces
the evaluation of the overlap to determine the distance between a point and
the circumference of the elliptical body. The simulation method was applied
to the motion in a rotary kiln and on a grate to proof its applicability to the
above-mentioned objectives. In particular, the results for the forward moving
grate showed, that the motion resembles a plug flow with little lateral mixing.

6 Literature

Beckmann M., Scholz R.; (2000).Residence time behaviour of solid material in grate system, In 5th European Conference on Industrial Furnaces and Boilers, Espinho-Porto, Portugal, April 11-14, 2000

Džiugys A., B. Peters, (1998). Numerical Simulation of the Motion of Granular Material. FZKA 6156. Forschungszentrum Karlsruhe GmbH, Karlsruhe, Germany, 1998.

Hunsinger H., J. Vehlow, B. Peters, H.H. Frey (2000). Performance of a pilot waste incinerator under different air/fuel ratios. In IT3 International Conference on Incineration and Thermal Treatment Technologies, Portland, Oregon, USA, May 8-12, 2000. CD-ROM, Irvine, Calif. : The Regents Univ. of California, 2000

Korn G.A., Korn T.M. (1968) Mathematical Handbook. McGraw-Hill Book Company, 1968.

Lin X., T.-T. Ng (1995). Contact detection algorithms for three-dimensional ellipsoids in discrete element modelling, International Journal for Numerical and Analytical Methods in Geomechanics, vol.19, pp. 653-659.

Lin X., T.-T. Ng (1997). A three-dimensional discrete element model using arrays of ellipsoids, Geotechnique, vol.47, No.2, pp. 319-329.

Peters B. (1996). Efficient software development and use for engineering applications with TOSCA (Tools of Object-oriented Software for Continuum Mechanics Applications), CFD 96, Fourth Annual Conference of the CFD Society of Canada, Ottawa, Ontario, Canada, June 2-4, 1996.

Peters B. (1997). Application de la conception object oriente a la modelisation de l'incineration de dechets municipaux. Geiger, W. [Hrsg.], Umwelt-informatik '97 : 11. Internat. Symp. der Gesellschaft für Informatik (GI), Strasbourg, F, September 10-12, 1997, Marburg : Metropolis-Verl., 1997 Vol. 2 S. 668-77 (Umwelt-Informatik aktuell ; Bd. 15)

Peters B., A. Džiugys (1998). Numerical Simulation of Particle Motion and Combustion in a Packed Bed, Lee, J. S. [Hrsg.], Heat Transfer 1998 : Proceedings of 11th International Heat Transfer Conference, Kyongju, Korea, August 23-28, 1998, Vol. 4: General Papers, pp. 277-282, Korean Society of Mechanical Engineers, 1998.

Peters B., A. Džiugys (1998b). Numerical Simulation of Particle Motion in a Packed Bed using Object-Oriented Techniques, International Conference on Numerical Methods for Fluid Dynamics, Institute for Computational Fluid Dynamics, Oxford, GB, March 31 - April 3, 1998, Baines, M. J. [Hrsg.],

Numerical Methods for Fluid Dynamics, Vol. 6, pp. 459-465, Oxford : Will Print, 1998

Rothenburg L., R.J. Bathurst (1991). Numerical simulation of idealized granular assemblies with plane elliptical particles, Computers and Geotechnics, vol.11, pp. 315-329.

Stroustrup B. (1991). The C++ Programming Language, Addison-Wesley Publishing Company.

Ting J.M. (1991). An ellipse-based micromechanical model for angular granular materials, in Proc.ASCE Engineering Mechanics Conference on Mechanics Computing in 1990' and Beyond, No.Part 2, ed. by Hojjat Adeli, Columbus, OH, pp. 1214-1218.

Ting J.M. (1992). A robust algorithm for ellipse-based discrete ellement modelling of granular material. Computers and Geotechnics, vol.13, No.3, pp. 175-186.

Ting J.M., M. Khwaja, L. Meachum, J.D. Rowell (1993). An ellipse-based discrete element model for granular materials, International Journal for Numerical and Analytical Methods in Geomechanics, vol.17, pp. 603-623.